HHS Public Access

Author manuscript

*J Med Chem*. Author manuscript; available in PMC 2024 June 22.

Published in final edited form as:

*J Med Chem*. 2023 June 22; 66(12): 7868–7879. doi:10.1021/acs.jmedchem.3c00238.

# A Serum-Stable Gold(III) Bisphosphine Complex Induces Mild Mitochondrial Uncoupling and In Vivo Antitumor Potency in Triple Negative Breast Cancer

**Adedamola S. Arojojoye**[a], **Chibuzor Olelewe**[a], **Sailajah Gukathasan**[a], **Jong H. Kim**[a], **Hemendra Vekaria**[d,e], **Sean Parkin**[a], **Patrick G. Sullivan**[d,e,f], **Samuel G. Awuah**[a,b,c]

[a]Department of Chemistry, University of Kentucky, Lexington KY 40506, USA.

[b]Center for Pharmaceutical Research and Innovation and Department of Pharmaceutical Sciences, College of Pharmacy University of Kentucky, Lexington KY 40536, USA

[c]Markey Cancer Center, University of Kentucky, Lexington KY 40536.

[d]Spinal Cord and Brain Injury Research Center, University of Kentucky, Lexington KY 40536, U.S.A.

[e]Department of Neuroscience, University of Kentucky, Lexington KY 40536, U.S.A.

[f]Department of Neuroscience, University of Kentucky Lexington KY 40536, U.S.A.

## Abstract

The preparation of cyclometalated complexes offers a path to stable materials, catalysts, and therapeutic agents. Here, we explore the anticancer potential of novel biphenyl organogold(III)

**Corresponding Author** Samuel G. Awuah, Department of Chemistry, College of Arts and Sciences, University of Kentucky, 505 Rose Street, Lexington, Kentucky 40506-0055, United States; Center for Pharmaceutical Research and Innovation and Department of Pharmaceutical Sciences, College of Pharmacy University of Kentucky, Lexington KY 40536, USA; Markey Cancer Center, University of Kentucky, Lexington KY 40536. awuah@uky.edu.

Author Contributions

Conceptualization, A.S.A. and S.G.A.; methodology, A.S.A.; synthesis and characterization, A.S.A.; X-ray crystallography, S.R.P.; Biological assays, A.S.A and C.O; APCI-MS studies A.S.A and S.G, Serum stability studies S.G and J.H.K, In vivo studies, C.O and J.H.K.; Seahorse assay and MMP studies A.S.A, H.V, P.G.S and S.G.A Electrochemistry, UV–vis spectrometry A.S.A, .; writing—original draft preparation, A.S.A. and S.G.A.; writing—review and editing, A.S.A and S.G.A.; supervision, S.G.A.; funding acquisition, S.G.A.

Conflicts of interest

The authors declare the following financial interests/personal relationships which may be considered as potential competing interests: Samuel G. Awuah has patents pending to University of Kentucky Research Foundation.

Supporting Information

The Supporting Information is available free of charge at

Crystal data and structure refinement for compounds **Au-1**, **Au-2**, **Au-2a**, **Au-3a**, (Table S1–S4, Fig S1-S4); $^{1}H$, $^{13}C$, $^{31}P$ spectra, HPLC traces, APCI-MS, Electrochemistry, and UV-Vis spectra for compounds **Au-1**–**Au-5** (Figures S1–S59); Dose response graphs for compounds **Au-1**–**Au-5** and cisplatin (Figure S60 – S65), Apoptosis Au-3 (Fig. S66), Standard curve for in vivo biodistribution of Au-3 (S69) Mitochondria membrane potential of isolated mitochondria of C57BL/6J mice treated with **Au-1** and **Au-2** using TMRE dye (S68-S69) Mitostress assay of cisplatin (S70), whole cell uptake of **Au1**-**Au-5** (S71)

Molecular formular strings



The authors declare no competing financial interest.

cationic complexes supported by diverse bisphosphine ligands, **Au-1**-**Au5**, towards aggressive glioblastoma and triple negative breast cancer cells (TNBCs). The [C^C] gold(III) complex, **Au-3** exhibits significant tumor growth inhibition in a metastatic TNBC mouse model. Remarkably, **Au-3** display promising blood serum stability over a relevant therapeutic window of 24 h and alteration in the presence of excess *L*-GSH. Mechanism-of-action studies show that **Au-3** induces mitochondrial uncoupling, membrane depolarization, G1 cell cycle arrest, and prompts apoptosis. To the best of our knowledge, **Au-3** is the first biphenyl gold-phosphine complex to uncouple mitochondria and inhibit TNBC growth in vivo.

## Graphical Abstract

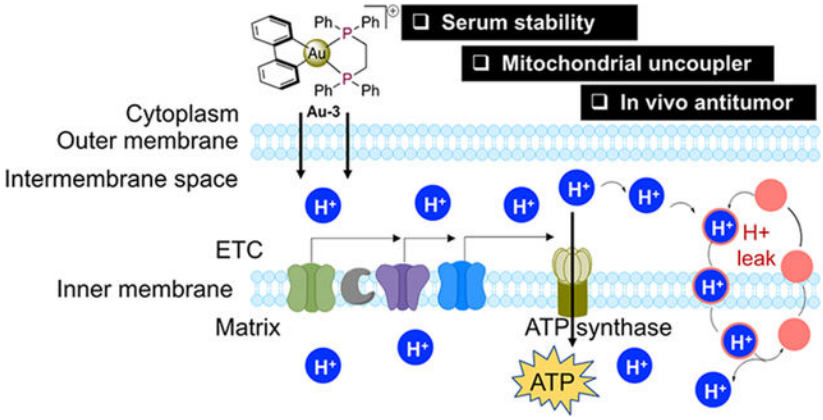


### Keywords

gold(III) complexes; bisphosphine; uncoupling; mitochondria; cyclometalation

## INTRODUCTION

Cancer remains one of the most difficult diseases to treat and is associated with high mortality rates.[1, 2] The spectrum of available effective drugs is still limited with some presenting acute toxicity and severe side effects,[3-5] therefore, developing new drugs and treatment options are desperately needed. Gold-based complexes represent a promising class of bioactive agents with remarkable anticancer potential.[6-8] Ongoing research towards repurposing auranofin for various diseased conditions in the clinic[9, 10] has stimulated the development and elucidation of different gold-derived anticancer agents and their mode of drug action.

Structural modifications to gold-containing scaffolds result in complexes manifested by changes in oxidation states, geometry, and different chelating ligands to stabilize the gold center.[11-17] Notable work include the development of mitochondrial targeting Au(I)-NHCs and Au(I)-$(DPPE)_2Cl$ that showed high cytotoxicity against cancer cells in vitro and in vivo but failed in preclinical toxicity studies.[18, 19] Furthermore, Au(III)-dithiocarbamate complexes triggers proteosome inhibition and potent in vivo effects.[20] Gold porphyrin is another class of Au(III) complexes with excellent cytotoxic profile in a panel of cancer

cells and inhibited tumor growth in mice with multiple mechanisms of action depending on the tetranitrogenic porphyrin ligand used.[21-24] To resolve the existing problem of Au(III) complex instability, we and others have used cyclometalation as a strategy to improve compound stability in solution.[25-29] Recent speciation studies using chiral Au(III) complexes with glutathione deepened our understanding into Au(III) stability, however enhanced complex stability will facilitate clinical translation of gold therapeutic agents.[30] The use of [C^C]-cyclometalation demonstrated stability for use as catalysts and as luminescent agents.[31-35] Recently, [C^C]Au(III) bearing bidentate ligands was shown to exhibit cytotoxic activity in cancer cells, however their biological target, and mechanism-of-action studies was not fully elucidated.[36]

Bisphosphines are diverse bidentate ligands that have found widespread use in coordination chemistry, homogeneous transition metal-catalyzed organic reactions, and in biological systems.[37] Early work on the preparation of cytotoxic gold complexes bearing bisphosphines, by Berners-Price, Sadler and Mirabelli[18, 38-41] followed by other synthetic efforts to develop bisphosphine-supported gold agents have highlighted their importance as possible chemotherapeutics.[42-47] Darkwa et al., and Raubenheimer et al., independently studied the effect of the nature of phosphine ligands on the anticancer properties of phosphinogold(I) complexes. They rationalized that the substituent on the phosphorus atom dictates the anticancer activity. Bisphosphine complexes with longer $CH_2$ linkers demonstrate better anticancer properties than complexes with shorter $CH_2$ linkers.[48, 49] However, their mechanism of cytotoxic action was not fully discussed.

Reducing the efficiency of energy conversion while maintaining high intracellular phosphate levels in the mitochondria is known as mitochondrial uncoupling.[50-53] Pharmacological induction of mild mitochondrial uncoupling has been used to control obesity, atherosclerosis, diabetes, fatty liver disease, and more recently cancer by dinitrophenol (DNP) and its derivatives.[50, 54-57] Thus, novel small-molecules that induce mitochondrial uncoupling can alter cancer cell metabolism, energy homeostasis, and mitochondria-dependent apoptosis towards clinically-relevant targeted therapy. Earlier reports on $[Au(I)\text{-}(DPPE)_2]^+$ has shown that they induce uncoupling of mitochondrial oxidative phosphorylation by enhanced permeability of the inner mitochondrial membrane to cations in isolated rat liver mitochondria.[58, 59] We hypothesized that stable redox-active Au(III) cations interact with mitochondria to enhance electron flux leading to mitochondrial uncoupling.

Here, we prepared biphenyl Au(III) complexes bearing bisphosphine ligands with significant serum and solution stability as well as mild mitochondrial uncoupling activity to disrupt mitochondrial energy states. The complexes possess potent anticancer activity in multiple aggressive cancer cells including TNBC and glioblastoma cells and inhibit TNBC tumor growth in vivo. To our prime knowledge, this is the first account of Au(III) complexes to induce mitochondrial uncoupling and inhibit tumor growth in vivo.

## Result and Discussion

### Synthesis and Characterization

We rationalized that the $\mu$-chloro biphenyl Au(III)[33, 60, 61] could be a readily accessible building block to preparing bisphosphine substituted organogold complexes of the archetype, [[C^C]Au(III)P-P]$^+$. The synthetic protocol is amenable to different bisphosphine ligands such as quinoxaline frameworks with or without chiral phosphanyl side chain (**Au-1** or **Au-4**) or aromatic backbone with aromatic phosphanyl side chain (**Au-2** and **Au-5**) and aromatic backbone with aliphatic phosphanyl side chains (**Au-3**) in moderate yields (Figure 1A).

All synthesized gold complexes were characterized by $^1$H NMR, $^{31}$ P NMR and $^{13}$C NMR, EA and purity accessed by HPLC and found to be greater than 97%. Single crystals of complexes were resolved by X-crystallography either with chloride anions (**Au-1**, **Au-2**) or [C^C]Au(III)Cl$_2$ anions (**Au-2a**, **Au-3a**) to elucidate the structure of the complexes (Figure 1B, Figure S1-S4). Electrochemical characterization of representative complexes (**Au-2** and **Au-3**) by cyclic voltammetry in acetonitrile revealed low redox potentials with a reduction peak at −1.14 V and oxidation events at 0.65 - 0.79 V using Ag/AgCl reference electrodes (Figure 1C, Figure S30-S33).

### Physiological Stability Studies

Evidence for physiological stability of **Au-1**–**Au-5** was established using systematic UV-vis spectroscopy, APCI-MS or LC-ESI-MS methods (Figure 2, Figure S34-S61). First, UV-vis spectroscopic monitoring of the reaction of the complexes (100 μM) with L-GSH (1000 μM) showed unaltered high energy charge transfer transitions over 24 hours for all complexes except **Au-5**. Complexes **Au-2** and **Au-3** show absorption peaks at ~250 nm and ~350 nm respectively over 24 hours. (Figure 2A, Figure 4B, Figure S41-S59). Further MS analysis of the reaction between *L*-GSH with **Au-1**- **Au-5** in an equimolar ratio by APCI-MS confirmed that no quantitative adduct was formed. For instance, **Au-2** and **Au-3** showed peaks that with m/z = 794.5 [**Au-2**] and 746.5 [**Au-3**] corresponding to [M-Cl]$^+$ peaks dominant after 8 h of reaction with no interaction with *L*-GSH (m/z = 307.8 (Figure 2A, Fig. S41-S59 ). Second, a more translational stability study was performed by incubating **Au-3** in murine blood serum for 24 h. Quantitative decay plots using LC-ESI-MS show that more than 60% of the complex remain intact suggesting that majority of **Au-3** may remain intact in circulation until it reaches its site of action (Figure 2B).

### In vitro Cytotoxicity and Cellular uptake

Several cyclometalated Au(III) complexes have been shown to induce significant antiproliferative activity by apoptosis or autophagy.[62-65] We expected that **Au-1**–**Au-5** recapitulate these features. **Au-1**–**Au-5** showed lower IC$_{50}$ values compared to cisplatin (a first line chemotherapeutic drug) in the panel of cancer cells studied: MDA-MB-468 and MDA-MB-231 (human breast cancer), 4T1 (murine breast cancer), and BT333 (human glioblastoma) 72 h posttreatment by MTT (Table 1, Figure S60-S65).

### Apoptosis and Cell Cycle Analysis

Evidence for apoptosis came from a fluorescence assisted cell sorting (FACS) study using the TNBC cells MDA-MB-468 cells exposed to 0.1 μM or 0.3 μM of **Au-3** along with Annexin-V-FITC and propidium iodide (Figure 3A). From the study it was inferred that cells treated with **Au-3** induced 17.4% and 31.6% apoptosis at 0.1 and 0.3 μM respectively in MDA-MB-468 cells after 48 h of exposure when compared to control cells. A similar trend was observed for MDA-MB-231 cells (Figure S66). To analyze the effect of **Au-3** on DNA content, FACS studies revealed marginal cell cycle arrest with an 8% increase of G0/G1 phase in MDA-MB-468 at 1 μM in a dose-dependent fashion after 12 h post treatment (Figure 3B). This finding coupled with our design principle of a stable lipophilic cation led us to suggest that **Au-3** may target mitochondria and disrupt metabolic pathways.

### Au-3 induces mitochondria uncoupling activity in TNBC cells.

Mitochondrial uncoupling can be characterized by key biochemical hallmarks including: (i) increase in oxygen consumption even at the inhibition of ATP synthase, ii) reduction in mitochondrial potential and iii) decrease in mitochondrial ATP production. These among others destabilize cellular energy homeostasis and create an exploitable vulnerability for relevant cancer treatment.

We initially tested whether **Au-3** would promote oxygen consumption rate (OCR) in a Mitostress test using Seahorse XF96. In isolated mitochondria from C57BL/6J mice, a concentration-dependent increase in OCR at state IV respiration (Figure 3C) was observed even when ATP synthase was inhibited by oligomycin indicative of uncoupling activity. Additionally, in cancer cells where the membrane potential is more negative to drive accumulation of lipophilic cation complexes such as **Au-3**, the complex induced increased OCR in MDA-MB-468 cells. As inferred from the maximal respiration in the presence of oligomycin (Figure 3D & 3E) and extrapolated proton leak (Figure 3F), significant increase in OCR up to 2.7 μM with concomitant decrease in coupling efficiency confirmed mitochondrial uncoupling (Figure 3G). The highest **Au-3** concentration of 8.3 μM induced stress in cancer cells that shut down the ETC compared to effects on healthy mitochondria, depicting selectivity.

Next, levels of respiratory-linked ATP were assessed in MDA-MB-468 cells incubated with **Au-3** compared to vehicle control cells. Following an initial burst in ATP production at 0.1 μM of **Au-3**, higher dose treatments of 1 μM – 8.3 μM resulted in total abrogation of ATP production, which is the energy currency of the cell (Figure 3H).

To test whether the mitochondria uncoupling activity induced by **Au-3** was independent of cytotoxic action or cellular stress, we investigated the uncoupling potential of the cytotoxic platinum drug, cisplatin in MDA-MB-468 cells. Briefly, cells were treated with varying concentrations of cisplatin for 12 h. Following the 12 h pre-treatment period, mitostress test was performed as previously described and we observed that cisplatin did not alter OCR significantly. Extrapolated maximal respiration, proton leak, and coupling efficiency data (Figure S70A-E) support this finding. Clearly, **Au-3**-induced mitochondria uncoupling

activity is differentiated from cisplatin and the characteristic uncoupling phenotype is consistent with the hypothesis put forth.

Another crucial phenotype of uncoupler-induced cytotoxicity is the loss of mitochondrial membrane potential ($\Delta\psi_m$). Using fluorescence-based assays, we assessed whether Au-3 depolarized $\Delta\psi_m$. **Au-3** induced depolarization in isolated mitochondria in a concentration-dependent manner from 0.1 μM – 2.7 μM along with TMRE (tetramethylrhodamine, ethyl ester), which labels active mitochondria via a plate-reader (Figure 3I). The depolarized phenotype was recapitulated in live MDA-MB-468 cells using JC-1 assay via microscopy. The treatment of MDA-MB-468 with 10 μM led to green JC-1 monomers, indicative of mitochondrial depolarization (Figure 3J).

## Structure Activity Relationship (SAR) Considerations

We further carried out a detailed structure activity relationship study on **Au-1**-**Au-5** to understand the effect of phosphanyl side groups and backbone on their cellular responses. First, theoretical LogP values of **Au1**-**Au-5** were computed using SWISSADME software.[68] **Au-1** with aliphatic t-butyl and methyl phosphanyl side groups displayed the lowest lipophilicity (LogP = 4.88) and **Au-2**-**Au-5** with phenyl side groups displayed high lipophilicity (LogP = 6.38 – >10). Although **Au-1** and **Au-4** differ only in the nature of side groups attached to the quinoxaline phosphanyl backbone, they display great differences in lipophilicity as shown in Figure 4A. Also, within complexes with phenyl side groups, **Au-3** with aliphatic non-conjugated backbone has the lowest LogP value while **Au-5** with increased conjugated binapthyl backbone displayed a LogP value greater than 10. Second, solution stability studies of **Au-1**-**Au-5** in DMEM or GSH also showed that complexes with aliphatic phosphanyl side group (**Au-1**) or backbone **Au-3** were more stable compared to complexes with conjugated phosphanyl side group and backbone (Figure 4B, Figure S34-S59).

We further evaluated SAR by measuring the intracellular accumulation of **Au-1**–**Au-5** in cancer cell lines. MDA-MB-468 cells were treated with **Au-1**–**Au-5** at 10 μM for 18 h and the intracellular accumulation of the compounds were determined by GF-AAS (Fig. 4C). Cellular uptake of all compounds was above 400 pmol per million cells except **Au-5** that displayed low intracellular accumulation. This was attributed to the increased conjugated binapthyl phosphanyl backbone of **Au-5** and limited solubility due to high lipophilicity. This result can further explain the higher $IC_{50}$ values measured for **Au-5** in the four cancer cell lines tested compared to **Au-1–Au-4** (Table 1). Also, **Au-3** with aliphatic ethane backbone showed the highest cellular uptake and corresponding low $IC_{50}$ values indicating that conjugation adversely impacts cellular uptake. To test the impact of the different phosphanyl groups on oxygen consumption rates and mitochondria membrane potential in isolated mitochondria from C57BL/6J mice **Au-1–Au-3** was chosen, and we observed a concentration dependent increase in OCR up to 8.3 μM with corresponding decrease in MMP. At a low concentration of 2.7 μM, **Au-3** displayed similar OCR levels comparable to **Au-1** and **Au-2** at a higher concentration of 8.3 μM showing that a low dose of **Au-3** is needed to induce uncoupling effect compared to **Au-1** or **Au-2 (**Figure 4D-F). Taken

together, these results validate the influence of phosphanyl backbone and/or side groups on biological activity imposed by this class of compounds.

## In vivo Anticancer activity

To illustrate the therapeutic impact on aggressive tumors, we assessed the efficacy of **Au-3** *in vivo* using a metastatic TNBC syngeneic model. Balb/c mice were injected with 4T1 murine TNBC cells subcutaneously (Figure 5A). The mice were administered intraperitoneally with **Au-3** at a dose of 10 mg/kg on alternate days, three times each week. Comparisons were made between the treatment group and a control group that received the vehicle (PBS solution containing 1% DMSO and 10% Kolliphor). We observed a significant tumor growth delay in 4T1 tumors; tumor growth inhibition measured at the end of the study was 36% (Figure 5B).

To assess preliminary toxicity of **Au-3**, we used body weight (Figure 5C). By the end of the study mice did not lose >5% of body weight, suggestive of optimal tolerability. Biodistribution studies show significant accumulation in kidneys and liver, which suggest that these organs may be the major clearance hubs of Au-3 (Figure 5D). Further, histological assessment to evaluate potential adverse effects by hematoxylin and eosin staining showed no signs of toxicity across all tissues examined (Figure 5E).

## Conclusions

In summary, we show that [C^C]-cyclometalated Au(III), **Au-3**, exhibits mitochondrial uncoupling and impressive potency against aggressive cancer cells. Moreover, **Au-3** display significant stability in blood serum, which is of clinical relevance and resist reduction from biological nucleophiles. Strikingly, the organometallic complex, **Au-3** inhibits metastatic TNBC tumor growth in mice. Presumably, this report is likely the first account of a gold-based organometallic complex with mitochondrial uncoupling and promising antitumor activity. Our study fortifies the therapeutic value of organometallic gold agents and specifically provides the framework for the development of safe metal-based uncouplers.

## Experimental Procedures

### General Information:

Solvents used in this work were purchased from Pharmco-Aaper (ACS grade) and they were used as purchased. $HAuCl_4 \cdot 3H_2O$ was purchased from Nano Partz and stored under nitrogen atmosphere. *S,S*-QuinoxP* was purchased from Strem Chemicals. 2,2-dibromobiphenyl was purchased from Matrix scientific. (±)-2,2′-Bis(diphenylphosphino)-1,1′-binaphthalene was purchased from Oakwood chemicals. 1,2-bis(diphenylphosphino)ethane and di-*n*-butyl tin dichloride was purchased from Alfa Aesar. 1,2-bis(diphenylphosphino)benzene was purchased from ChemScene. *N*-BuLi and anhydrous ether was purchased from Sigma Aldrich. 3-(4,5-dimethylthiazol-2-yl)-2,5-diphenyltetrazolium bromide (MTT) was purchased from Cayman Chemicals. $\mu$-chloro biphenyl Au(III) [33, 60, 61] and 2,3-bis(diphenylphosphino)quinoxaline[37] were synthesized according to reported procedures. Deuterated solvents were purchased from Cambridge Isotope Laboratories (Andover, MA).

NMR spectra were recorded on a Bruker Avance NEO 400 MHz spectrometer and 500 MHz JEOL ECZr. Samples were calibrated for: $^{1}$H NMR ($CDCl_3$ δ = 7.26 ppm), $^{13}$C($^{1}$H-decoupled) NMR ($CDCl_3$ δ = 77.16), and $^{31}$P($^{1}$H-decoupled) NMR externally referenced to $H_3PO_4$ $\delta$ = 0.00). High-resolution mass spectra (HRMS) were obtained by direct flow injection (injection volume = 2 μL) using ElectroSpray Ionization (ESI) on a Waters Synapt G2 HDMS instrument in the positive mode with a quadrupole/TOF analyzer (UC Boulder). Elemental analysis results were obtained from Atlantic Microlabs, Inc (Norcross, GA). In addition to spectroscopic characterization, the purity of all compounds was assessed by RP-HPLC using an Agilent Technologies 1100 series HPLC instrument and an Agilent Phase Eclipse Plus C18 column (4.6 mm x 100 mm; 3.5 μm particle size). All compounds were found to be >97% pure. Fluorescent images were obtained from fluorescence microscope in total internal reflection fluorescence (TIRF) and epifluorescence mode using 488 and 510 nm laser excitation, power 1 mW/cm$^2$ exposure time of 200 milliseconds using 20X air objective. Images were processed with ImageJ software.

## Synthesis and Characterization

**General Procedure for the Preparation of [Au-C^C-P^P] compounds:** In a 50 mL round-bottom flask with stir bar was added 7 mL of chloroform and $\mu$-chloro biphenyl Au(III) (1.0 equiv.). The corresponding bisphosphine ligand (1.0 equiv.) was added. The solution was stirred at room temperature and monitored with TLC to show completion of reaction. The reaction was then purified on combiflash using 10% MeOH/DCM, precipitated from diethyl ether to afford the desired solid products.

**Synthesis of Au-1:** Prepared as described in the general procedure. $\mu$-chloro biphenyl Au(III) (30 mg, 0.039 mmol) and S,S-Quinox P* (13.04 mg, 0.039 mmol). Yield: 8.5 mg, 32 % $^{1}$H NMR (400 MHz, $CDCl_3$) δ (ppm) 8.44 (dd, 4 Hz, 2H), 8.17 (dd, 8 Hz, 2H), 7.83-7.88 (m, 2H), 7.55 – 7.57 (dq, 2H), 7.32 (t, 8 Hz, 2H), 7.19 (t, 8 Hz, 2H), 2.70 (d, 8 Hz, 6H), 1.22 (d, 16 Hz, 18H). $^{13}$C NMR (101 MHz, $CDCl_3$): δ (ppm)155.60, 155.59, 155.58, 153.34, 152.83, 143.68, 143.65, 143.61, 137.59, 137.52, 137.45, 135.32, 130.72, 129.43, 129.01, 128.87, 123.46, 123.44, 123.41, 37.36, 37.25, 37.14, 28.35, 28.33, 28.31, 6.20, 6.09, 6.06, 5.95. $^{31}$P NMR (161.9 MHz, $CDCl_3$): δ(ppm) 44.34 APCI-MS (found) = 682.6 $[M\text{-}Cl]^+$ (calculated) = 683.2 Anal. Calcd: $C_{30}H_{36}AuClN_2P_2$: C, 50.12%; H, 5.05% Found: $C_{30}H_{36}AuClN_2P_2 \cdot 0.5\ C_4H_{10}O$: C, 50.81% H, 5.48%. Purity was determined to be > 97% by RP-HPLC: $R_f$ = 10.6 minutes using the following method: Flow rate: 1 mL/min; λ = 280 nm; Eluent A = DI water with 0.1% trifluoroacetic acid; Eluent B = Acetonitrile with 0.05% formic acid; Solvent Gradient: 0 – 16 min (0:100 $H_2O$: ACN). 16 min until end of run (100:0 $H_2O$: ACN).

**Synthesis of Au-2:** Prepared as described in the general procedure. $\mu$-chloro biphenyl Au(III) (40 mg, 0.05 mmol) and 1,2-Bis(diphenylphosphino)benzene (23.22 mg, 0.05 mmol) Yield : 20 mg, 47% 1H NMR (500 MHz, CDCl3): δ (ppm) 7.87 (dd, 10 Hz 2H), 7.63 (dd, 15 Hz, 8H), 7.50-7.56 (m, 8H), 7.39-7.43 (m, 8H), 7.05-7.16 (m, 4H), 6.58 (t, 10 Hz, 2H) 13C NMR (125.7 MHz) δ (ppm)121.01, 122.88, 122.93, 124.39, 124.90, 124.91, 126.79, 127.10, 128.14, 128.21, 128.27, 128.60, 130.18, 130.24, 130.30, 133.31, 133.58, 133.65, 134.86, 134.92, 134.98, 135.18, 135.22, 135.26, 136.00, 136.07, 136.15, 136.27,

136.34, 136.42, 137.91, 137.97, 138.18, 138.49, 138.64 138.76, 154.98, 155.01, 162.03, 162.10, 163.18, 163.25 $^{31}$PNMR (202.4 MHz) δ (ppm) 51.65 APCI-MS (found) = 794.5 $[M-Cl]^+$ (calculated) = 795.16. Anal. Calc. $C_{42}H_{32}AuClP_2$ C, 60.7%, H, 3.88% Found: $C_{42}H_{32}AuClP_2 \cdot 0.65\ CH_2Cl_2$ C, 57.73% H 3.69%. Purity was determined to be > 97% by RP-HPLC: $R_f$ = 9.77 minutes using the following method: Flow rate: 1 mL/min; λ = 280 nm; Eluent A = DI water with 0.1% trifluoroacetic acid; Eluent B = Acetonitrile with 0.05% formic acid; Solvent Gradient: 0 – 16 min (0:100 $H_2O$: ACN). 16 min until end of run (100:0 $H_2O$: ACN).

**Synthesis of Au-3:** Prepared as described in the general procedure. *μ*-chloro biphenyl Au(III) (60 mg, 0.078 mmol) and 1,2-Bis(diphenylphosphino)ethane (31.08 mg, 0.078 mmol). Yield : 21 mg, 34.4 %. $^1$H NMR (500 MHz, CDCl3): δ 7.82 (dd, 15, 10 Hz, 8H), 7.63 (t, 5 Hz, 4H), 7.56 (t, 5 Hz, 8H), 7.51 (t, 5 Hz, 2H), 7.12 (q, 10 Hz, 4H, 6.62 (t, 10 Hz, 2H), 3.31-3.42 (m, 4H), 13C NMR (125.7 MHz) δ 29.71, 30.0, 122.39, 122.45, 122.77, 123.28, 128.41, 128.70, 130.23, 130.35, 133.52, 134.17, 134.29, 137.40, 137.54, 155.05, 161.68, 161.74, 162.80, 162.87 $^{31}$PNMR (202.4 MHz) δ 60.39 APCI-MS (found) = 746.5 $[M-Cl]^+$ (calculated) = 747.16 Anal. Calcd: $C_{38}H_{32}AuClP_2$: C, 58.29%; H, 4.12% Found: C, 57.16%, H, 4.2% $C_{38}H_{32}AuClP_2 \cdot 0.85H_2O$ Purity was determined to be > 97% by RP-HPLC: $R_f$ = 10.3 minutes using the following method: Flow rate: 1 mL/min; λ = 280 nm; Eluent A = DI water with 0.1% trifluoroacetic acid; Eluent B = Acetonitrile with 0.05% formic acid; Solvent Gradient: 0 – 16 min (0:100 $H_2O$: ACN). 16 min until end of run (100:0 $H_2O$: ACN).

**Synthesis of Au-4:** Prepared as described in the general procedure. *μ*-chloro biphenyl Au(III), (40 mg, 0.05 mmol and 1,2-bis(diphenylphosphino)quinoxaline (24.95 mg, 0.05 mmol). Yield : 27 mg, 58.7 % 1H NMR (500 MHz, CDCl3): δ 8.11 (dd 10, 5Hz 2H), 7.85-7.90 (m, 10H), 7.49 (d, 5 Hz, 2H), 7.44 (t, 10 Hz, 4H), 7.33 (t, 5 Hz, 7H), 7.19 (m, 2H), 7.10 (t, 10 Hz, 2 H), 6.97 (t, 5 Hz, 0.5H), 6.74 (t, 10 Hz, 0.5H), 6.57 (t, 5H, 2H). 13C NMR (125 MHz, CDCl3) 120.43, 122.28, 122.31, 122.33, 123.33,123.41, 123.66, 123.68, 123.93, 124.01, 126.25, 126.49, 127.49, 127.56, 127.63, 127.83, 129.02, 129.21, 129.27, 129.32, 129.50, 130.21, 132.52, 133.04, 133.20, 135.50, 135.56, 135.61, 136.10, 136.18, 136.26, 142.79, 142.83, 152.21, 154.53, 154.92, 155.51, 156.02, 156.10, 160.54, 161.61 $^{31}$P NMR (202.4 MHz, $CDCl_3$) δ (ppm) 33.98 APCI-MS (found) = 846.5 $[M-Cl]^+$ (calculated) = 847.17 Elemental Analysis Anal. Calcd: $C_{44}H_{32}AuClN_2P_2$ C, 59.84%; H, 3.65%; Found: $C_{44}H_{32}AuClN_2P_2 \cdot 1.85H_2O \cdot 0.1C_4H_{10}O$; C, 57.7% H, 3.99% Purity was determined to be > 97% by RP-HPLC: $R_f$ = 10.77 minutes using the following method: Flow rate: 1 mL/min; λ = 280 nm; Eluent A = DI water with 0.1% trifluoroacetic acid; Eluent B = Acetonitrile with 0.05% formic acid; Solvent Gradient: 0 – 16 min (0:100 $H_2O$: ACN). 16 min until end of run (100:0 $H_2O$: ACN).

**Synthesis of Au-5:** Prepared as described in the general procedure. *μ*-chloro biphenyl Au(III), (40 mg, 0.05 mmol and (±)-2,2′-Bis(diphenylphosphino)-1,1′-binaphthalene (32.3 mg, 0.05 mmol). Yield : 18 mg, 34.3 % $^1$H NMR (500 MHz, CDCl3): δ 8.26 (d, 5 Hz, 2H), 7.75 – 7.82 (m, 3H), 7.59 (d, 10Hz, 4H), 7.53 (t, 5 Hz, 2H), 7.43 (t, 10 Hz, 6H), 7.37 (d, 10 Hz, 2H), 7.21 (d, 5 Hz, 4H), 7.15 (t, 10 Hz, 2H), 6.97 - 7.02 (m, 6H), 6.82 (t,

5 Hz, 2H), 6.70 (d, 10 Hz, 2H), 6.50 (q, 10 Hz, 2H), 6.33 ( t, 10 Hz, 2H) $^{13}$CNMR (175 MHz, CDCl3) δ 156.02, 154.38, 152.31, 140.02, 139.95, 139.91, 136.45, 136.38, 136.31, 135.62, 135.52, 134.68, 134.61, 134.39, 134.31, 134.09, 133.28, 133.24, 133.03, 132.98, 132.85, 132.84, 132.78, 131.81, 130.61, 130.58 130.55, 130.50, 129.23, 129.16, 128.81, 128.75, 128.69, 128.50, 128.40, 128.31, 128.11, 128.08, 128.05, 128.01, 127.91, 127.69, 127.57, 127.49, 127.44, 127.35, 126.52, 126.50, 126.30, 125.80, 124.75, 122.39, 122.37, 120.42, 119.25, 119.17 $^{31}$P NMR (202.4 MHz) δ (ppm) 35.46 APCI-MS (found) = 970.4 $[M-Cl]^+$ (calculated) = 971.23 Elemental Analysis Anal. Calcd. $C_{56}H_{40}AuClP_2$ C, 66.77% H, 4.0% Found: $C_{56}H_{40}AuClP_2$ $C_{56}H_{40}AuClP_2 \cdot 1.35\ CH_2Cl_2$ C, 61.49% H, 3.66% Purity was determined to be > 97% by RP-HPLC: $R_f$ = 11.56 minutes using the following method: Flow rate: 1 mL/min; λ = 280 nm; Eluent A = DI water with 0.1% trifluoroacetic acid; Eluent B = Acetonitrile with 0.05% formic acid; Solvent Gradient: 0 – 16 min (0:100 $H_2O$: ACN). 16 min until end of run (100:0 $H_2O$: ACN).

## Physical and Chemical Characterization

**X-ray Crystallography.—**Diethylether was slowly diffused into concentrated solutions of **Au-1, Au-2a** and **Au-3a** in dichloromethane at room temperature while **Au-2** was grown in slow diffusion of $Et_2O$ into a concentrated solution of $CDCl_3$. Solid crystals were carefully examined under a microscope and mounted using polyisobutene oil on the end of a glass fibre, which had been mounted to a copper pin using an electrical solder. It was placed directly in the cold gas stream of a liquid nitrogen cryostat[69, 70] A Bruker D8 Venture diffractometer with graded multilayer focused MoKα X-rays (λ = 0.71073 Å) was used to collect diffraction. Raw data were integrated, scaled, merged, and corrected for Lorentz-polarization effects using the APEX3 package.[71-73] Space group determination and structure solution and refinement were carried out with SHELXT and SHELXL respectively.[74, 75] All non-hydrogen atoms were refined with anisotropic displacement parameters. Hydrogen atoms were placed at calculated positions and refined using a riding model with their isotropic displacement parameters (Uiso) set to either 1.2Uiso or 1.5Uiso of the atom to which they were attached. Ellipsoid plots were drawn using SHELXTL-XP.[76] The structures, deposited in the Cambridge Structural Database, were checked for missed symmetry, twinning, and overall quality with PLATON,[77] an R-tensor,[78] and finally validated using CheckCIF.[77]

**Cyclic Voltammetry of Au-2 and Au-3.—**Electrochemical measurements of the ligands were recorded with a scan rate of 0.1 V/s with a three-segment sweep and a sample interval of 0.001 V. For complexes **Au-2** and **Au-3** further characterization was performed by scanning at different rates (0.05 V/s, 0.1 V/s, 0.2V/s, and 0.3 V/s). The quiet time was set to 2 seconds and sensitivity 1 $x10^{-4}$ A/V. All solutions were freshly prepared prior to use. All spectra were recorded using a CH instruments 650E potentiostat. The electrodes used were all 3 mm: glassy carbon working electrode (CHI104), Ag/AgCl reference electrode (CHI111), and a platinum wire counter electrode (CHI115). Both compounds **Au-2** and **Au-3** as well as both free ligands were prepared as a 5 mM solution in dry MeCN with $NBu_4PF_6$ (0.1 M) as the supporting electrolyte. The samples were purged with nitrogen for 30 minutes and recorded. Data were analyzed with GraphPad Prism 9.5.

**Reactivity with GSH (UV-vis Spectroscopy).—**Stock solutions of the complexes were prepared by dissolving appropriate amount of compound and making a 1 mM solution in DMSO. The stock solutions were diluted down to 100 μM with DI $H_2O$. A separate stock solution of GSH was prepared as a 1 mM stock x 5 mL. All spectra were recorded on a Shimadzu UV-1280 model instrument. Prior to each recording the instrument was blanked. The 1:10 solutions of the complex (100 μM) and GSH (1000 μM) were mixed, and the UV-vis spectra recorded at the indicated time intervals. For each reaction, the spectrum was normalized to the highest absorbance and plotted in GraphPad Prism 9.5.

**Reactivity with GSH (LC-MS Analysis).—**Stock solutions of the complexes were prepared by dissolving appropriate amount of compound and making a 1 mM stock solution in acetonitrile and the solution was diluted to 100 μM. A separate stock solution of GSH was prepared as a 10 mM stock and diluted to 100 μM. A 1:1 solution of the complex **Au-1** - **Au-5** (100 μM) and GSH (100 μM) were mixed, and the solution was then subjected to APCI-MS analysis using an Agilent 1200 HPLC with a direct flow injection with a HPLC auto sampler without a column, λ = 280 nm, (injection volume: 40 μL, flow rate: 0.2 mL/ min). ESI positive mode was taken with a source temperature of 120 °C, desolvation temperature of 300 °C, Capillary Vat 3.5 kV while Cone was set at 35. Results were taken at 0 h, 1h, 4 h, and 8 h interval. Data was plotted and analyzed using Mestrenova.

## In Vitro Biological Characterization

**Cell Culture.—**Cancer cell lines (MDA-MB-231, MDA-MB-468, 4T1 and BT-333) used in this study were purchased from ATCC. MDA-MB-231, MDA-MB-468, and BT-333 were grown in DMEM supplemented with 10% FBS, 1% amphotericin and 1% penicillin/ streptomycin in a humidified incubator at 37 °C with 5-10% $CO_2$. The 4T1 cells were grown in RPMI supplemented with 10% FBS, 1% amphotericin, and 1% penicillin / streptomycin, and 4 mM glutamine.

**Cell Viability of complexes.—**The cytotoxicity assay of **Au-1**-**Au-5** and **cisplatin** was performed using 3-(4,5-dimethylthiazol-2-yl)-2,5-diphenyltetrazolium bromide assay (MTT assay) in MDA-MB-231, MDA-MB-468, BT-333 and 4T1 cancer cells. After the cells had reached confluency Trypsin was added to detach and harvest the cells. The cells were washed in PBS and suspended in 10 mL of DMEM (or RPMI for 4T1 cells). The cells were centrifuged at 2000 rpm for five minutes, media decanted and resuspended in 5 mL of the appropriate medium. The cells were plated in a 96-well clear bottom plate at a density of 4,000 cells per well and left to adhere overnight at 37 °C with 5-10% $CO_2$. **Au-1**–**Au-5** and cisplatin were prepared as a stock in DMSO and PBS respectively and added at seven different concentrations starting at 100 μM for the highest concentration with a 3x serial dilution for subsequent wells and incubated at 37 °C for 72 h with 5-10% $CO_2$. After 72 h, the media was removed and replaced with a solution of MTT (100 μL, prepared by dissolving MTT at 5 mg/mL and diluting by 10x with DMEM) was added to each well and incubated for 4h at 37 °C with 5-10% $CO_2$. The dye was removed from each well and 100 μL of DMSO was added to induce cell lysis. The plates were read using a Genios plate reader (λ = 570 nm). The experiment was performed in triplicate and data are plotted as the

mean ± s.e.m. (n = 3). Data can be found in the main text and the other complexes can be seen in the supplementary figures.

**Whole Cell Uptake Analysis:** MDA-MB-468 cells (1 x $10^6$) were seeded in a 6 well plate and allowed to adhere overnight at 37 °C. Cells were treated with compound for 18 h, collected via trypsinization, centrifuged at 2000 rpm for 5 minutes to form a pellet. The pellet was suspended in 1 mL of DMEM, transferred to 1.5 mL Eppendorf tube and centrifuged at 2000 rpm for 5 minutes. The media was removed, and pellets resuspended and washed in PBS (1 ml x 2) and stored at −20 °C until further analysis. Prior to analysis, pellet was suspended in 70 % HNO3 200 μL, digested for 4 h, allowed to cool to room temperature and diluted appropriated before been analyzed on GF-AAS. Cellular gold concentration was expressed as pmol of Au per million cells.

**Apoptosis Analysis.—**MDA-MB-231 cells were seeded at a density of 5 x $10^5$ cells/well in a 6 well clear bottom plate with a final media volume of 2 mL. The cells were allowed to adhere overnight at 37 °C. A stock of **3** was prepared fresh in DMSO and added to the desired well at a concentration of 1 μM with a final volume of 2.5 mL and incubated for 4 h at 37 °C. A stock of H2O2 was prepared in PBS and the cells treated at a final concentration of 2 mM for 1 hour as a positive control. When ready for analysis, the media were removed, and the wells washed with 5 mL of PBS. The cells were trypsinized (1 mL), 5 mL of DMEM were added to each well, and total volume collected and centrifuged to pellet the cells. The cells were resuspended in 2 mL of fresh media, counted, and reconstituted to a concentration of 1 x $10^5$ cells/mL. The cells were centrifuged again, and the pellet suspended in 500 μL of Annexin binding buffer. To each sample was added 5 μl of Annexin V-FITC and 5 μl PI and incubated in the dark at room temperature for 5 minutes. The samples were then subjected to FACS analysis. Graphs are representative of three technical replicates.

**MDA-MB-468 Mitochondria Respiration Analysis.—**MDA-MB-468 cells (30,000 cells per well) were seeded in a XF96 Seahorse plate and allowed to adhere overnight in an incubator at 37 °C with 5-10% $CO_2$. **Au-3** and cisplatin was prepared as stock solution in DMSO and PBS respectively and diluted to 75 μM with Seahorse XF96 assay buffer and then subsequently serial diluted by 3x to achieve multiple concentrations and added for 12 h prior to measurement on the XF96 Seahorse. This was followed by injection of oligomycin (1.5 μM), FCCP (0.6 μM) and rotenone/ antimycin A (0.5 μM). The metabolic parameters were calculated from the reading gotten from a minimum of 6 wells.

**Cell Cycle Analysis.—**MDA-MB-468 cells were seeded at a density of 2 x $10^5$ cells/well in a 6 well clear bottom plate with a final media volume of 2 mL and allowed to adhere overnight 37 °C. **Au-3** was prepared fresh as a stock in DMSO and added at a concentration of 0.5 μM and 1 μM with a final volume of 2.5 mL for 12 h. After 12 h, the medium was removed and added to a 15 mL Falcon tube. The wells were washed with PBS (5 mL), trypsinized (1 mL) and 5 mL of fresh DMEM was added. All media were combined, and the tube centrifuged at 2000 rpm for 5 minutes to collect the pellet. The pellet was resuspended in 1 mL of PBS, and transferred to a 1 mL Eppendorf tube, centrifuged at 2000 rpm for 5

minutes, decanted and resuspended in 70% EtOH/PBS solution. This solution was stored at 4 °C until ready for analysis. Prior to analysis, the stored cells were collected by centrifuging at 2000 rpm for 5 minutes, washed twice with PBS (1 mL) and resuspended in a 50 μL of RNase solution (100 mg/mL) and 200 μL of a 50 mg/mL PI solution. The solutions were then filtered through a 5 mL round polystyrene bottom tube fit with a cell-strainer cap. The samples were then analyzed with FACS. Data are representative of three technical replicates with percentages plotted as the mean ± s.e.m. (n = 3).

## Animal Experiment

### Mouse Liver Mitochondrial Membrane Potential.

Differential mitochondrial isolation method was used to isolate mouse liver mitochondria were isolated from 8–9-week-old mouse. 10μg mito were run on HTX plate reader containing 100μl Respiration buffer. The Membrane potential was monitored using TMRE dye (150 nM final concentration). Compounds **Au-3** was dissolved in DMSO to make 25mM stock solutions. The stocks were further diluted 1:10 in DMSO to prepare working stock 2.5 mM. The working stock was serially diluted (5 times) 1:3 in DMSO to prepare further dilutions 0.83 mM, 0.27 mM, 0.09 mM, 0.03 mM and 0.01 mM. 1μl of each of these dilutions were added to reaction well containing respiration buffer to have final concentrations of the compound as 25μm, 8.3μM, 2.7μM, 0.9μM, 0.3μM and 0.1μM respectively. Results for 25 μM and 8.3 μM not included. The plate was read at λ= 530ex/590em with the mito, and subsequently after addition of pyruvate+Malate, Oligomycin and FCCP. The difference (Δ) between FCCP-Oligomycin were taken as a maximum membrane potential difference between the coupled and uncoupled states of respiration.

### Mouse Liver Mitochondria Respiration using Seahorse.

Mouse Liver mitochondria isolated from 8–9-week-old C57BL/6 mouse using differential mito isolation was used for this study. 5μg mito per well were run on Seahorse (XFe96) containing Respiration buffer. Compounds **Au-3** was dissolved in DMSO to make 25 mM stock solutions. The stocks were further diluted 1:10 in DMSO to prepare stock of 2.5mM. The working stock was serially diluted (5 times) 1:3 in DMSO to prepare further dilutions (each of 100X) 0.83mM, 0.27mM, 0.09mM, 0.03mM and 0.01mM. 16 μl of each of these dilutions (100X) were added to 186 μl respiration buffer and 25 μl was added to reaction well containing respiration buffer to have final concentrations of the compound as 25 μm, 8.3 μM, 2.7 μM, 0.9 μM, 0.3 μM and 0.1 μM respectively. The Oxygen consumption rates (OCR) were monitored after compound addition during top up volume (25 μl) followed by pyruvate+malate+ADP, oligomycin, FCCP and rotenone+succinate addition through injection ports A, B, C and D respectively and measuring OCR after each addition.

### In vivo experiment:

5-week-old female BALB/c mice were purchased from Jackson Laboratories and quarantined for a period of one week before inoculation with 1,000,000 4T1 cells subcutaneously on their right flanks. After 3 days of implantation, the mice were systemically treated with 10 mg/kg **Au-3** via intraperitoneal administration. **Au-3** was formulated in DMSO (1%), Kolliphor (10%), and PBS (89%) and delivered at 100 μL. The

control group was treated with a PBS solution containing 1% DMSO and 10% Kolliphor. The injection of **Au-3** was performed three times a week for two weeks. Tumor size and body weight measurements were performed three days a week, and mice were euthanized 15 days later. All mice were maintained in a pathogen-free environment under the care of DLAR of University of Kentucky. Our study was performed in compliance with the NIH guidelines (NIH Publication No. 85-23 Rev. 1985) for the care and use of laboratory animals and all experimental procedures were monitored and approved by the Institutional Animal Care and Use Committee (IACUC) of University of Kentucky (USA).

### Hematoxylin and eosin (H&E) staining.

The mice used in the in vivo comparative experiment of **Au-3** were sacrificed at day 14 post tumor cells(4T1) injection. Freshly prepared paraformaldehyde (4% in PBS) was used to fix harvested mice organs (heart, lung, liver, kidney, spleen, and tumor) for 24 h before been processed for paraffin sectioning. The organs sections of 5 μm were stained with H&E staining and used for histological examination of the organs and tumor. A total of 5 sections per tissue (spanning the full depth of the organ) were examined and photographed using a Nikon Eclipse 55i microscope.

### Tissue biodistribution.

Tissues obtained from the in vivo studies were used for tissue biodistribution. The tissues were boiled for 5 hours at 60 °C with 70% $HNO_3$ (0.5 ml) and then boiled again at 60 °C for 10 minutes by adding 35% hydrogen peroxide (0.5 ml). The solution turned yellow and diluted as needed to measure the gold content using a Graphite Furnace Atomic Absorption Spectrometer. Before measuring all samples, the standard solution curves were measured.

### Serum Stability.

Blood samples were taken from 14 weeks old BALB/cJ female mice and used for serum stability. Au-3 was prepared as a 100 mM stock solution in DMSO. 2.5 μL of Au-3 was taken and mixed with 247.5 μL of serum to make a final volume of 250 μL. For the experiment, serum containing Au-3 (17 μL) was mixed with MeOH (80 μL ). The solution was vortexed for 1 minute and centrifuged at 14,000 rpm at 4 °C for 10 minutes. The clear supernatants were taken and subjected to LCMS analysis at different time points (0, 10, 30, 60, 120, 360, and 1440 min). The result was plotted as the % of Au-3 serum stability against time. All experiments were performed in duplicate.

## Supplementary Material

Refer to Web version on PubMed Central for supplementary material.

## Acknowledgements

We are grateful for financial support from the National Cancer Institute (NCI) R01CA258421-01 (S.G.A.).

We would like to thank the following facilities at the University of Kentucky who provided support in completion of the experiments detailed in this manuscript. The UK NMR Center supported by NSF (CHE-997738) and the UK X-ray facility supported by the MRI program from NSF (CHE-1625732). For the flow cytometry experiments we would like to thank UK Flow Cytometry and Immune Function core supported by the Office of the Vice President

of Research, the Markey Cancer Center, and NCI Center Core Support Grant (P30 CA177558). We thank Dr. Chris Richard's lab for access and assistance with fluorescence microscopy. We would also like to thank Dr. Steven Van Lanen's lab for access to their APCI-MS.

## Abbreviations used

| | |
|---|---|
| **APCI-MS** | atmospheric pressure chemical ionization mass spectrometry |
| **ATP** | adenosine triphosphate |
| **AUC** | area under the curve |
| **DMEM** | dulbecco's modified eagle medium |
| **DNP** | dinitrophenol |
| **DPPE** | 1,2-Bis(diphenylphosphino)ethane |
| **ESI** | electrospray ionization |
| **FBS** | fetal bovine serum |
| **GF-AAS** | graphite furnace atomic absorption spectrometry |
| **HPLC** | high performance liquid chromatogram |
| **L-GSH** | L-glutathione |
| **MMP** | mitochondria membrane potential |
| **NHC** | N-heterocyclic carbine |
| **ORTEP** | oak ridge thermal ellipsoid plot |
| **PBS** | phosphate buffer saline |
| **TMRE** | tetramethylrhodamine, ethyl ester |
| **TNBC** | triple negative breast cancer |

## References

(1). Siegel RL; Miller KD; Wagle NS; Jemal A Cancer statistics, 2023. CA Cancer J. Clin 2023, 73 (1), 17–48. [PubMed: 36633525]

(2). Chhikara BS; Parang K Global Cancer Statistics 2022: the trends projection analysis. Chem. Biol. Lett 2023, 10 (1), 451–451.

(3). Schlichtig K; Dürr P; Dörje F; Fromm MF New oral anti-cancer drugs and medication safety. Dtsch Arztebl Int 2019, 116 (46), 775. [PubMed: 31920193]

(4). Williams AM; Liu Q; Bhakta N; Krull KR; Hudson MM; Robison LL; Yasui Y Rethinking success in pediatric oncology: beyond 5-year survival. J. Clin. Oncol 2021, 39 (20), 2227. [PubMed: 33769834]

(5). Yeh JM; Ward ZJ; Chaudhry A; Liu Q; Yasui Y; Armstrong GT; Gibson TM; Howell R; Hudson MM; Krull KR Life expectancy of adult survivors of childhood cancer over 3 decades. JAMA oncology 2020, 6 (3), 350–357. [PubMed: 31895405]

(6). Yue S; Luo M; Liu H; Wei S Recent advances of gold compounds in anticancer immunity. Front. Chem 2020, 8, 543. [PubMed: 32695747]

(7). Fernández-Moreira V; Herrera RP; Gimeno MC Anticancer properties of gold complexes with biologically relevant ligands. Pure Appl. Chem 2019, 91 (2), 247–269.

(8). Mertens RT; Gukathasan S; Arojojoye AS; Olelewe C; Awuah SG Next Generation Gold Drugs and Probes: Chemistry and Biomedical Applications. Chem. Rev 2023. DOI: 10.1021/acs.chemrev.2c00649.

(9). Yamashita M. Auranofin: Past to Present, and repurposing. Int. Immunopharmacol 2021, 101, 108272. [PubMed: 34731781]

(10). Liu Y; Lu Y; Xu Z; Ma X; Chen X; Liu W Repurposing of the gold drug auranofin and a review of its derivatives as antibacterial therapeutics. Drug Discov. Today 2022.

(11). Olelewe C; Kim JH; Ofori S; Mertens RT; Gukathasan S; Awuah SG Gold (III)-P-chirogenic complex induce mitochondrial dysfunction in triple-negative breast cancer. iScience 2022, 104340.

(12). Gukathasan S; Awuah SG Synthetic Strategies for the Preparation of Gold-based Anticancer Agents. EIBC 2011, 1–32.

(13). Bao M; Zhou S; Hu W; Xu X Recent advances in gold-complex and chiral organocatalyst cooperative catalysis for asymmetric alkyne functionalization. Chin.Chem.Lett 2022.

(14). Lu Y; Ma X; Chang X; Liang Z; Lv L; Shan M; Lu Q; Wen Z; Gust R; Liu W Recent development of gold (I) and gold (III) complexes as therapeutic agents for cancer diseases. Chem. Soc. Rev 2022.

(15). Mulks FF Gold carbene complexes and beyond: new avenues in gold (I)-carbon coordination chemistry. Gold Bull. 2022, 55 (1), 1–13.

(16). Arojojoye AS; Mertens RT; Ofori S; Parkin SR; Awuah SG Synthesis, Characterization, and Antiproliferative Activity of Novel Chiral [QuinoxP* AuCl2]+ Complexes. Molecules 2020, 25 (23), 5735. [PubMed: 33291802]

(17). Gurba A; Taciak P; Sacharczuk M; Młynarczuk-Biały I; Bujalska-Zadrożny M; Fichna J Gold (III) derivatives in colon cancer treatment. Int. J. Mol. Sci 2022, 23 (2), 724. [PubMed: 35054907]

(18). Berners-Price SJ; Mirabelli CK; Johnson RK; Mattern MR; McCabe FL; Faucette LF; Sung C-M; Mong S-M; Sadler PJ; Crooke ST In vivo antitumor activity and in vitro cytotoxic properties of bis [1, 2-bis (diphenylphosphino) ethane] gold (I) chloride. Cancer Res. 1986, 46 (11), 5486–5493. [PubMed: 3756897]

(19). Hickey JL; Ruhayel RA; Barnard PJ; Baker MV; Berners-Price SJ; Filipovska A Mitochondria-targeted chemotherapeutics: the rational design of gold (I) N-heterocyclic carbene complexes that are selectively toxic to cancer cells and target protein selenols in preference to thiols. J. Am. Chem. Soc 2008, 130 (38), 12570–12571. [PubMed: 18729360]

(20). Nardon C; Schmitt SM; Yang H; Zuo J; Fregona D; Dou QP Gold (III)-dithiocarbamato peptidomimetics in the forefront of the targeted anticancer therapy: Preclinical studies against human breast neoplasia. PLoS One 2014, 9 (1), e84248. [PubMed: 24392119]

(21). Chow KH-M; Sun RW-Y; Lam JB; Li CK-L; Xu A; Ma D-L; Abagyan R; Wang Y; Che C-M A gold (III) porphyrin complex with antitumor properties targets the Wnt/β-catenin pathway. Cancer Res. 2010, 70 (1), 329–337. [PubMed: 19996284]

(22). Che C-M; Sun RW-Y; Yu W-Y; Ko C-B; Zhu N; Sun H Gold (III) porphyrins as a new class of anticancer drugs: cytotoxicity, DNA binding and induction of apoptosis in human cervix epitheloid cancer cells. Chem. Commun 2003, (14), 1718–1719.

(23). Sun RW-Y; Che C-M The anti-cancer properties of gold (III) compounds with dianionic porphyrin and tetradentate ligands. Coord. Chem. Rev 2009, 253 (11-12), 1682–1691.

(24). Wang Y; He QY; Che CM; Chiu JF Proteomic characterization of the cytotoxic mechanism of gold (III) porphyrin 1a, a potential anticancer drug. Proteomics 2006, 6 (1), 131–142. [PubMed: 16287165]

(25). Zou T; Lum CT; Lok C-N; Zhang J-J; Che C-M Chemical biology of anticancer gold (III) and gold (I) complexes. Chem. Soc. Rev 2015, 44 (24), 8786–8801. [PubMed: 25868756]

(26). Oberkofler J; Aikman B; Bonsignore R; Pöthig A; Platts J; Casini A; Kühn FE Exploring the Reactivity and Biological Effects of Heteroleptic N-Heterocyclic Carbene Gold (I)-Alkynyl Complexes. Eur. J. Inorg. Chem 2020, 2020 (11-12), 1040–1051.

(27). Di Sarra F; Fresch B; Bini R; Saielli G; Bagno A Reactivity of auranofin with selenols and thiols–implications for the anticancer activity of gold (I) compounds. Eur. J. Inorg. Chem 2013, 2013 (15), 2718–2727.

(28). Yangyuoru PM; Webb JW; Shaw CF III Glutathionato-S-Gold (III) complexes formed as intermediates in the reduction of auricyanide by glutathione. J. Inorg. Biochem 2008, 102 (3), 584–593. [PubMed: 18255156]

(29). Đurović MD; Bugarčić ŽD; Heinemann FW; van Eldik R Substitution versus redox reactions of gold (III) complexes with L-cysteine, L-methionine and glutathione. Dalton Trans. 2014, 43 (10), 3911–3921. [PubMed: 24448551]

(30). Arojojoye AS; Kim JH; Olelewe C; Parkin S; Awuah SG Chiral gold (III) complexes: speciation, in vitro, and in vivo anticancer profile. 2022, 58 (73), 10237–10240.

(31). Nilakantan L; McMillin DR; Sharp PR Emissive biphenyl cyclometalated gold (III) diethyl dithiocarbamate complexes. Organometallics 2016, 35 (14), 2339–2347.

(32). David B; Monkowius U; Rust J; Lehmann C; Hyzak L; Mohr F Gold (III) compounds containing a chelating, dicarbanionic ligand derived from 4, 4′-di-tert-butylbiphenyl. Dalton Trans. 2014, 43 (28), 11059–11066. [PubMed: 24919777]

(33). Usón R; Vicente J; Cirac J; Chicote M Synthesis and reactivity of dibenzometallole complexes of gold (III) and platinum (II). J. Organomet. Chem 1980, 198 (1), 105–112.

(34). Joost M; Estévez L; Miqueu K; Amgoune A; Bourissou D Oxidative addition of carbon–carbon bonds to gold. Angew. Chem., Int. Ed 2015, 127 (17), 5325–5329.

(35). Wu C-Y; Horibe T; Jacobsen CB; Toste FD Stable gold(III) catalysts by oxidative addition of a carbon–carbon bond. Nature 2015, 517 (7535), 449–454. DOI: 10.1038/nature14104. [PubMed: 25612049]

(36). Khodjoyan S; Remadna E; Dossmann H; Lesage D; Gontard G; Forté J; Hoffmeister H; Basu U; Ott I; Spence P [(C C) Au (N N)]+ Complexes as a New Family of Anticancer Candidates: Synthesis, Characterization and Exploration of the Antiproliferative Properties. Chem. Eur. J 2021, 27 (63), 15773–15785. [PubMed: 34436799]

(37). Adam MSS; Mohamad AD; Jones PG; Kindermann MK; Heinicke JW Comparison of the reactivity of 2-amino-3-chloro-and 2, 3-dichloroquinoxalines towards Ph2PH and Ph2PLi and of the properties of diphenylphosphanyl-quinoxaline P, N and P, P ligands. Polyhedron 2013, 50 (1), 101–111.

(38). Mirabell CK; Johnson RK; Hill DT; Faucette LF; Girard GR; Kuo GY; Sung CM; Crooke ST Correlation of the in vitro cytotoxic and in vivo antitumor activities of gold (I) coordination complexes. J. Med. Chem 1986, 29 (2), 218–223. [PubMed: 3081721]

(39). Mirabelli CK; Hill DT; Faucette LF; McCabe FL; Girard GR; Bryan DB; Sutton BM; Barus JOL; Crooke ST; Johnson RK Antitumor activity of bis (diphenylphosphino) alkanes, their gold (I) coordination complexes, and related compounds. J. Med. Chem 1987, 30 (12), 2181–2190. [PubMed: 3681888]

(40). Berners-Price SJ; Sadler PJ Gold (I) complexes with bidentate tertiary phosphine ligands: formation of annular vs. tetrahedral chelated complexes. Inorg. Chem 1986, 25 (21), 3822–3827.

(41). Berners-Price SJ; Girard GR; Hill DT; Sutton BM; Jarrett PS; Faucette LF; Johnson RK; Mirabelli CK; Sadler PJ Cytotoxicity and antitumor activity of some tetrahedral bis (diphosphino) gold (I) chelates. J. Med. Chem 1990, 33 (5), 1386–1392. [PubMed: 2329559]

(42). Carlos Lima J; Rodriguez L Phosphine-gold (I) compounds as anticancer agents: general description and mechanisms of action. Anti-Cancer Agents Med. Chem 2011, 11 (10), 921–928.

(43). Caruso F; Rossi M; Tanski J; Pettinari C; Marchetti F Antitumor activity of the mixed phosphine gold species chlorotriphenylphosphine-1, 3-bis (diphenylphosphino) propanegold (I). J. Med. Chem 2003, 46 (9), 1737–1742. [PubMed: 12699391]

(44). Higginbotham ML; Henry CJ; Katti KV; Casteel SW; Dowling PM; Pillarsetty N Preclinical tolerance and pharmacokinetic assessment of MU-Gold, a novel chemotherapeutic agent, in laboratory dogs. Veterinary ther. 2003, 4 (1), 76–82.

(45). Dennis EK; Kim JH; Parkin S; Awuah SG; Garneau-Tsodikova S Distorted Gold (I)–Phosphine Complexes as Antifungal Agents. J. Med. Chem 2019, 63 (5), 2455–2469. [PubMed: 31841324]

(46). Kim JH; Reeder E; Parkin S; Awuah SG Gold (I/III)-phosphine complexes as potent antiproliferative agents. Sci. Rep 2019, 9 (1), 1–18. [PubMed: 30626917]

(47). Olelewe C; Kim JH; Ofori S; Mertens RT; Gukathasan S; Awuah SG Gold(III)-P-chirogenic complex induces mitochondrial dysfunction in triple-negative breast cancer. iScience 2022, 25 (5), 104340. [PubMed: 35602949]

(48). Keter FK; Guzei IA; Nell M; Zyl W. E. v.; Darkwa J Phosphinogold (I) dithiocarbamate complexes: effect of the nature of phosphine ligand on anticancer properties. Inorg. Chem 2014, 53 (4), 2058–2067. [PubMed: 24476103]

(49). Horvath UE; Dobrzańska L; Strasser CE; Bouwer W; Joone G; van Rensburg CEJ; Cronje S; Raubenheimer HG Amides of gold (I) diphosphines prepared from N-heterocyclic sources and their in vitro and in vivo screening for anticancer activity. J. Inorg. Biochem 2012, 111, 80–90. [PubMed: 22498717]

(50). Demine S; Renard P; Arnould T Mitochondrial uncoupling: a key controller of biological processes in physiology and diseases. Cells 2019, 8 (8), 795. [PubMed: 31366145]

(51). Kotova EA; Antonenko YN Fifty years of research on protonophores: Mitochondrial uncoupling as a basis for therapeutic action. Acta Naturae 2022, 14 (1), 4.

(52). Hirschenson J; Melgar-Bermudez E; Mailloux RJ The uncoupling proteins: a systematic review on the mechanism used in the prevention of oxidative stress. Antioxidants 2022, 11 (2), 322. [PubMed: 35204205]

(53). Ardalan A; Smith MD; Jelokhani-Niaraki M Uncoupling Proteins and Regulated Proton Leak in Mitochondria. Int. J. Mol. Sci 2022, 23 (3), 1528. [PubMed: 35163451]

(54). Goedeke L; Shulman GI Therapeutic potential of mitochondrial uncouplers for the treatment of metabolic associated fatty liver disease and NASH. Molecular metabolism 2021, 46, 101178. [PubMed: 33545391]

(55). Shrestha R; Johnson E; Byrne FL Exploring the therapeutic potential of mitochondrial uncouplers in cancer. Molecular Metabolism 2021, 51, 101222. [PubMed: 33781939]

(56). Čater M; Bombek LK Protective Role of Mitochondrial Uncoupling Proteins against Age-Related Oxidative Stress in Type 2 Diabetes Mellitus. Antioxidants 2022, 11 (8), 1473. [PubMed: 36009191]

(57). Bonanno JA; Shyam R; Choi M; Ogando DG The H+ transporter SLC4A11: Roles in metabolism, oxidative stress and mitochondrial uncoupling. Cells 2022, 11 (2), 197. [PubMed: 35053313]

(58). Hoke GD; Rush G; Bossard G; McArdle J; Jensen BD; Mirabelli C Mechanism of alterations in isolated rat liver mitochondrial function induced by gold complexes of bidentate phosphines. J. Biol. Chem 1988, 263 (23), 11203–11210. [PubMed: 2457018]

(59). Hoke GD; Macia RA; Meunier PC; Bugelski PJ; Mirabelli CK; Rush GF; Matthews WD In vivo and in vitro cardiotoxicity of a gold-containing antineoplastic drug candidate in the rabbit. Toxicol. Appl. Pharmacol 1989, 100 (2), 293–306. [PubMed: 2781559]

(60). Chan KT; Tong GSM; Wan Q; Cheng G; Yang C; Che CM Strongly Luminescent Cyclometalated Gold (III) Complexes Supported by Bidentate Ligands Displaying Intermolecular Interactions and Tunable Emission Energy. Chem. Asian J 2017, 12 (16), 2104–2120. [PubMed: 28586132]

(61). Wu C-Y; Horibe T; Jacobsen CB; Toste FD Stable gold (III) catalysts by oxidative addition of a carbon–carbon bond. Nature 2015, 517 (7535), 449–454. [PubMed: 25612049]

(62). Babak MV; Chong KR; Rapta P; Zannikou M; Tang HM; Reichert L; Chang MR; Kushnarev V; Heffeter P; Meier-Menches SM; Lim ZC; Yap JY; Casini A; , W. H. Interfering with Metabolic Profile of Triple-Negative Breast Cancers Using Rationally Designed Metformin Prodrugs. Angew. Chem., Int. Ed 2021, 60 (24), 13405–13413.

(63). Huang K-B; Wang F-Y; Tang X-M; Feng H-W; Chen Z-F; Liu Y-C; Liu Y-N; Liang H Organometallic gold (III) complexes similar to tetrahydroisoquinoline induce ER-stress-mediated apoptosis and pro-death autophagy in A549 cancer cells. J. Med. Chem 2018, 61 (8), 3478–3490. [PubMed: 29606001]

(64). Zhang J; Zhang Z; Jiang M; Li S; Yuan H; Sun H; Yang F; Liang H Developing a novel gold (III) agent to treat glioma based on the unique properties of apoferritin nanoparticles: inducing lethal autophagy and apoptosis. J. Med. Chem 2020, 63 (22), 13695–13708. [PubMed: 33185442]

(65). Alhoshani A; Sulaiman AA; Sobeai HMA; Qamar W; Alotaibi M; Alhazzani K; Monim-ul-Mehboob M; Ahmad S; Isab AA Anticancer activity and apoptosis induction of Gold (III) complexes containing 2, 2′-bipyridine-3, 3′-dicarboxylic acid and dithiocarbamates. Molecules 2021, 26 (13), 3973. [PubMed: 34209921]

(66). Yang W; Soares J; Greninger P; Edelman EJ; Lightfoot H; Forbes S; Bindal N; Beare D; Smith JA; Thompson IR Genomics of Drug Sensitivity in Cancer (GDSC): a resource for therapeutic biomarker discovery in cancer cells. Nucleic Acids Res. 2012, 41 (D1), D955–D961. [PubMed: 23180760]

(67). Stompor M; Świtalska M; Wietrzyk J The influence of a single and double biotinylation of xanthohumol on its anticancer activity. Acta Biochim. Pol 2019, 66 (4), 559–565. [PubMed: 31820895]

(68). Daina A; Michielin O; Zoete V SwissADME: a free web tool to evaluate pharmacokinetics, drug-likeness and medicinal chemistry friendliness of small molecules. Sci. Rep 2017, 7 (1), 42717. [PubMed: 28256516]

(69). Parkin S; Hope H Macromolecular Cryocrystallography: Cooling, Mounting, Storage and Transportation of Crystals. J. Appl. Crystallogr 1998, 31 (6), 945–953. DOI: doi:10.1107/S0021889898005305.

(70). Hope H. X-ray crystallography - a fast, first-resort analytical tool. Prog. Inorg. Chem 1994, 41, 1–19. DOI: 10.1002/9780470166420.ch1.

(71). Bruker. “APEX2” Bruker-AXS; 2006.

(72). Krause L; Herbst-Irmer R; Sheldrick GM; Stalke D Comparison of silver and molybdenum microfocus X-ray sources for single-crystal structure determination. J Appl Crystallogr 2015, 48 (Pt 1), 3–10. DOI: 10.1107/S1600576714022985. [PubMed: 26089746]

(73). Sheldrick GM SADABS, Program for bruker area detector absorption correction.; 1997.

(74). Sheldrick GM Crystal structure refinement with SHELXL. Acta Crystallogr C Struct Chem 2015, 71 (Pt 1), 3–8. DOI: 10.1107/S2053229614024218. [PubMed: 25567568]

(75). Sheldrick GM SHELXT - integrated space-group and crystal-structure determination. Acta Crystallogr A Found Adv 2015, 71 (Pt 1), 3–8. DOI: 10.1107/S2053273314026370. [PubMed: 25537383]

(76). Sheldrick G. A short history of SHELX. Acta Crystallographica Section A 2008, 64 (1), 112–122. DOI: doi:10.1107/S0108767307043930.

(77). Spek AL Structure validation in chemical crystallography. Acta Crystallogr D Biol Crystallogr 2009, 65 (Pt 2), 148–155. DOI: 10.1107/S090744490804362X. [PubMed: 19171970]

(78). Parkin S. Expansion of scalar validation criteria to three dimensions: the R tensor. Erratum. Acta Crystallogr A 2000, 56 (Pt 3), 317. [PubMed: 10927222]

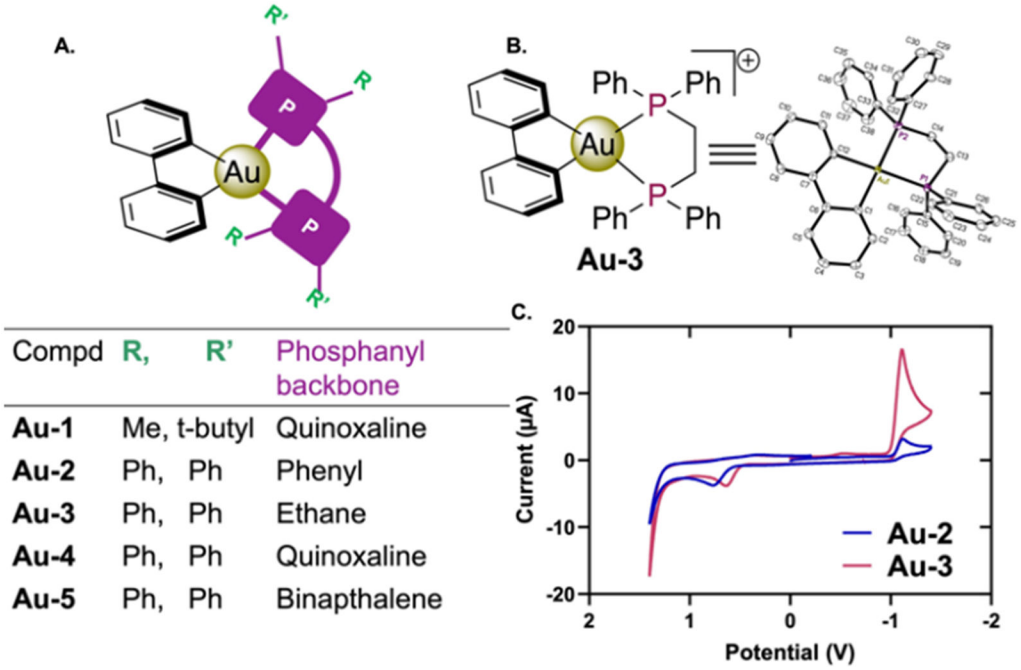


| Compd | R, | R' | Phosphanyl backbone |
|---|---|---|---|
| **Au-1** | Me, t-butyl | | Quinoxaline |
| **Au-2** | Ph, | Ph | Phenyl |
| **Au-3** | Ph, | Ph | Ethane |
| **Au-4** | Ph, | Ph | Quinoxaline |
| **Au-5** | Ph, | Ph | Binapthalene |

**Figure 1.**

A. Generic chemical structure of biphenyl Au(III) complexes showing bisphosphine ligands used in this work **B.** Chemical structure of **Au-3** used in this work and the ORTEP representation of **Au-3** (biphenyl $AuCl_2$ anion omitted for clarity). CCDC no: 2233442 **C.** Cyclic voltammogram of **Au-2** and **Au-3** at 0.1 V/s with Ag/AgCl reference electrode.

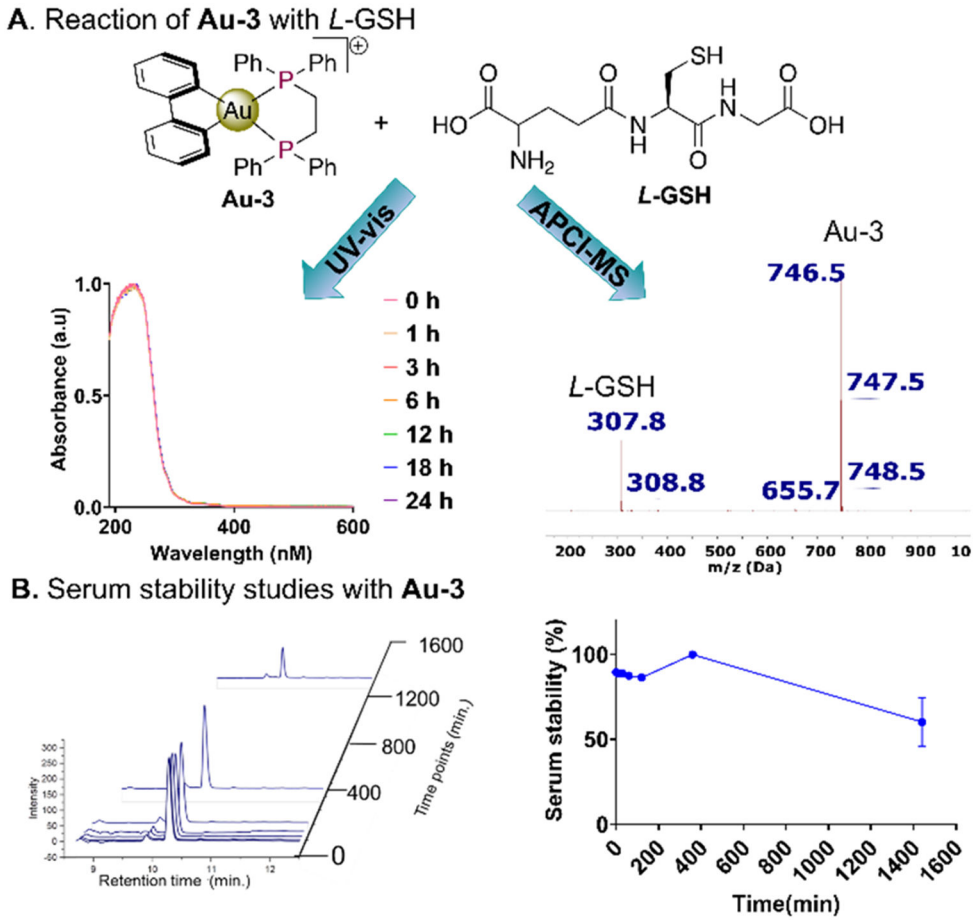


**Figure 2.**

Physiological stability studies. **A**. Reaction of **Au-3** with *L*-glutathione using UV-Vis (24 h) and APCI-MS (8 h) **B**. LC-ESI-MS serum stability studies of **Au-3** (100 μM, 24 h) and decay plot (right) extrapolated from HPLC AUC (left).

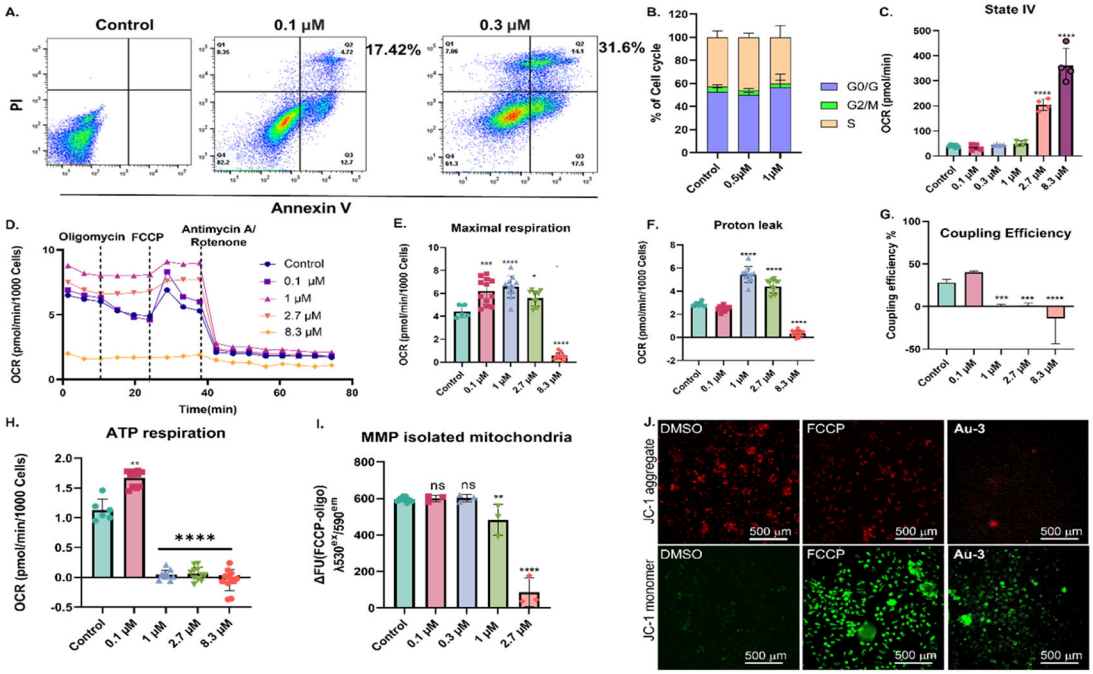


**Figure 3.**

Mechanistic studies on the mode of action of **Au-3. A**. Flow cytometry result showing apoptosis at 0.1 and 0.3 µM in MDA-MB-468 cells. **B**. Cell cycle analysis of **Au-3** at 0.5 and 1 µM. **C**. Extrapolated state IV data from isolated mitochondria of C57BL/6J mice. **D**. MitoStress study using Seahorse assay. MDA-MB-468 cancer cells were pretreated with **Au-3** (12 h) and various inhibitors of ETC were added at indicated time points. **E** to **H**. Key parameters extrapolated from Seahorse assay. **I**. Mitochondria membrane potential of isolated mitochondria of C57BL/6J mice using TMRE dye. **J**. Mitochondria membrane potential of MDA-MB-468 using JC-1 dye. **Au-3** was administered at (10 µM) for 90 minutes. Ordinary one-way ANOVA * p< 0.05, ** p< 0.1, *** p<0.001, ****p< 0.0001

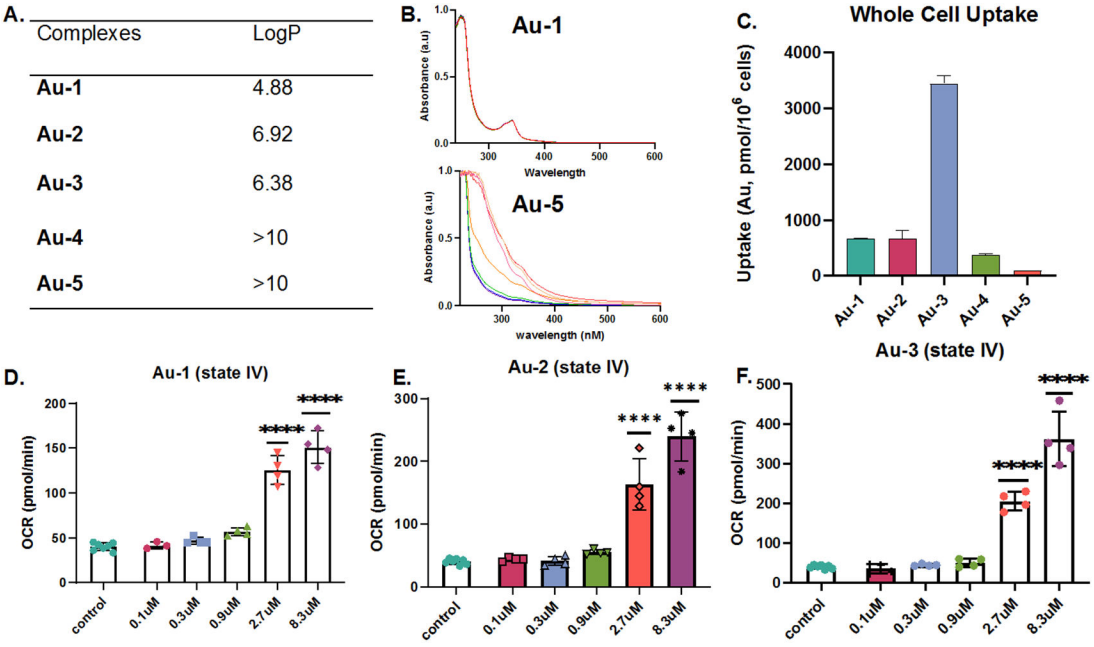


**Figure 4.**

Structure activity relationship studies. **A.** Theoretical LogP values of **Au-1**-**Au-5** computed from SWISSADME software. **B.** UV-Vis solution stability studies of **Au-1** (top) and **Au-5** (bottom) over 24 h. **C.** Intracellular accumulation of **Au1**-**Au-5** in MDA-MB-468 cancer cells. Cells were treated with 10 μM for 18 h. **D-F.** Extrapolated state IV data from treatment of **Au-1**-**Au-3** on isolated mitochondria of C57BL/6J mice. Ordinary one-way ANOVA * p< 0.05, ** p< 0.1, *** p<0.001, ****p< 0.0001

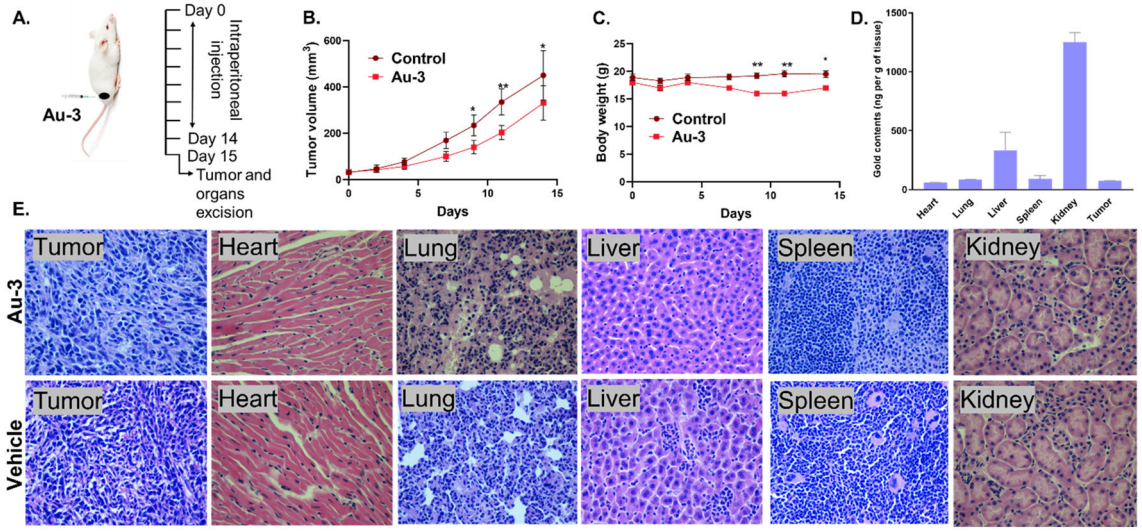


**Figure 5.**

Therapeutic potential of **Au-3**. **A**. Schematic diagram showing **Au-3** dosing schedule. **B** and **C.** Effect of **Au-3** on tumor volume and weight of 4T1 infected Balb/c mice. Unpaired t-test, *p< 0.05, **p< 0.01. **D**. Histology (H&E) staining of harvested tissue and tumor. **E**. Tissue biodistribution of **Au-3** determined by GF-AAS (n= 3).

**Table 1.**

Table showing $IC_{50}$ values (μM) for complex **Au-1**-**Au-5** and cisplatin, in MDA-MB-468, MDA-MB-231, 4T1 and BT-333 cancer cells.

| Compounds | MDA-MB-468 | MDA-MB-231 | 4T1 | BT-333 |
|---|---|---|---|---|
| Au-1 | 0.11± 0.12 | 0.49 ± 0.06 | 0.85 ± 0.18 | 0.76± 0.08 |
| Au-2 | 0.21± 0.14 | 0.25 ± 0.21 | 1.18 ± 0.16 | 0.93± 0.09 |
| Au-3 | 0.11± 0.09 | 0.55 ± 0.09 | 0.38 ± 0.2 | 0.52± 0.07 |
| Au-4 | 0.33± 0.18 | 0.20 ± 0.18 | 0.13 ± 0.08 | 1.43± 0.12 |
| Au-5 | 6.76± 0.65 | 2.62 ± 0.25 | 2.07 ± 0.27 | 3.38± 0.04 |
| cisplatin | 2.60± 0.61 | 43.14± 0.9[a] | 1.0 ± 0.17[b] | 23.2± 0.29 |

[a,b]Reported $IC_{50}$ values of cisplatin in MDA-MB-231 and 4T1.[66,67]